Int J Soc Robot (2012) 4:107–119
DOI 10.1007/s12369-011-0128-5

Stiffness and Impedance Control Using Lyapunov Theory for Robot-Aided Rehabilitation

Haifa Mehdi · Olfa Boubaker

Accepted: 20 November 2011 / Published online: 7 December 2011

Abstract In this paper, stiffness and impedance control concepts are used to solve position and force control for robot-aided rehabilitation. New asymptotic stability conditions are proposed using a suitable Lyapunov approach and based on the relationship between the dynamics of the robot and its energy. The efficiency of the proposed approach is tested on a planar 3 DOF robot-aided rehabilitation constrained to a circular trajectory. The robotic device is configured to be safe and stable in compliant motion in contact with the human arm. It is also designed to be adapted easily to different subjects for performing different tasks. Force and control parameters are tuned using a non linear optimization strategy for which the stability conditions are considered as inequality constraints. Simulation results show that the robot could guide the upper limb of subjects in circular movements under predefined model of the external force and prove the stability and the performances of the compliant motion control strategy.

Keywords Stiffness control · Impedance control · Lyapunov theory · Robot-aided rehabilitation

1 Introduction

Stroke is one of the leading causes of disability [1, 2]. To perform activities of daily living, all stroked patients require rehabilitation treatment necessitating labor and intensive leading efforts by the physiotherapists. Several robotic devices are currently developed for upper limbs assisting [3–6] and for lower limbs assisting [7, 8]. Research to date has shown that interactive treatment of the impaired limbs can serve as an objective and reliable means of monitoring patient progress by assisting them in moving the limb through a predetermined trajectory during a given motor task [9]. It is also revealed that repetitive task-specific, goal-directed, robot-assisted therapy is effective in reducing motor impairments in the affected arm after stroke [10]. Furthermore, most upper-limb rehabilitation robotic systems have 2DOF with planar motion for more therapy efficiency.

On the other hand, control system accomplishment is one of the major difficulties in rehabilitation robot design. Different approaches were developed to control movement of robot-aided therapy attached to human limbs. They can be classified into three categories: force control [4, 11], position control [6, 12], position and force control [13, 14]. The main difficulties occur for the last case, specially, when intending to realize predefined complex movements such as circular motion.

Several strategies and schemes were already proposed to solve the position and force control for robotic systems [15–22]. However, unlike industrial robots, rehabilitation-aided robots must be configured for stable, safe and compliant motion in contact with humans. The impedance control strategy proposed by Hogan [18, 19] is one of the most appropriate approaches for such applications. This approach is privileged for its simplicity. The objective of this control concept is to accomplish specific mechanical impedance at the manipulator end-effector [23]. So, the manipulator controller is designed to track a motion trajectory and realize a desired dynamic relationship between the end-effector position and the contact force. On the other hand, stiffness control initially proposed by Salisbury [17] can be

H. Mehdi · O. Boubaker (✉)
National Institute of Applied Sciences and Technology (INSAT), Centre Urbain Nord BP, 676-1080 Tunis Cedex, Tunisia
e-mail: olfa.boubaker@insat.rnu.tn

H. Mehdi
e-mail: Haifa.mehdi@gmail.com

also suitable to solve such position and force control problems. In fact, Stiffness control can be regarded as a special case of impedance control with only static model-based compensation [24].

Stability conditions for robotic systems under impedance or stiffness controllers had been investigated in many researches. This problem had been solved using linearized models [25–27]. Further analyses are done on the basis of nonlinear models [28–31]. Robust stability was also proposed in [32, 33]. However, in our best knowledge, the relation between the dynamics of the robot and its energy was never already exploited in this framework.

In this paper, we present then new asymptotic stability conditions for stiffness and impedance controllers using a suitable Lyapunov approach based on the relationship between the dynamics of the robot and its energy. The main contribution of this work is not only to build a specific control law providing stable compliant motion and sufficient contact force of the robot in contact with the stroked limb but also to supply satisfactory safety by allowing adaptability of the robotic device to different stroked patients and supporting their progress in the therapy process. In this paper, safety is guaranteed since some of the controller parameters can be adapted to different stroked patients and for different states of progression in the therapy process. The remaining controller parameters are finely tuned using a constrained nonlinear optimization strategy using the optimization toolbox of MatLab software.

The efficiency of the proposed approach is tested, by simulations on a planar 3 DOF robot-aided rehabilitation attached to a human upper limb. The physical parameters of the stroked arm are computed using the famous Winter statistical model.

The paper is organized as follows: In second section, the mathematical problem of robotic system in contact with the upper human arm through a force display is formulated. The new stability conditions of the stiffness and the impedance controllers are derived in the third and the fourth sections, respectively. In the fifth section, the design of a robot-aided rehabilitation is proposed, the controller parameters are optimized and the simulation results are performed.

2 Mathematical Formulation

Consider a robotic system with n degrees of freedom described in the joint space by the following dynamical model [24]:

$$M(\theta)\ddot{\theta} + H(\theta,\dot{\theta}) + G(\theta) = U - J(\theta)^T F \tag{1}$$

and the following forward kinematic models:

$$X = f(\theta) \tag{2a}$$

$$\dot{X} = J(\theta)\dot{\theta} \tag{2b}$$

where $\theta, \dot{\theta}, \ddot{\theta} \in R^n$ are joint position, velocity and acceleration vectors, respectively. $M(\theta) \in R^{n\times n}$ is the inertia matrix, $H(\theta,\dot{\theta}) \in R^n$ is the vector of centrifugal and Coriolis forces and $G(\theta) \in R^n$ is the vector of gravity terms. $U \in R^n$ is the generalized joint force vector, $F \in R^p$ is the vector of contact generalized forces exerted by the manipulator on the environment and p is the task space dimension. $J(\theta) \in R^{p\times n}$ is the Jacobian matrix and $X, \dot{X} \in R^p$ are position and velocity of the robotic system in the Cartesian space, respectively. The problem to be solved is to design control laws $U \in R^n$ satisfying asymptotic stability of the robotic system described by the dynamical model (1) and the kinematic models (2) under the following assumptions:

(a) The entire vectors of force, position, velocity and acceleration are measured.
(b) All feedback gains, used to solve the control problem are diagonal matrix with equal elements.

3 Stiffness Control

Stiffness control is designed to achieve a desired static behavior of the interaction of a robot manipulator with the environment [19]. The block diagram of the entire control system can be described as shown in Fig. 1.

Based on Fig. 1, the control law is given by:

$$U = J^T[K_p(X_d - X) + K_v(\dot{X}_d - \dot{X})] + G \tag{3}$$

where $K_p, K_v \in R^{p\times p}$ are position and velocity gain matrices, respectively.

In stiffness control, the joint stiffness matrix is modulated to achieve the desired relation between position and applied force [34]:

$$F = K_e(X_d - X) \tag{4}$$

where $K_e \in R^{p\times p}$ is the stiffness matrix of the system robot/environment.

3.1 Relationship Between the Dynamics of the Robotic System and Its Energy for Stiffness Control

Let Φ and $Y(\Phi)$ the errors in the joint space and in the task space of the robotic system defined respectively by:

$$\Phi = \theta - \theta_d \tag{5}$$

$$Y(\Phi) = X(\theta) - X_d \tag{6}$$

Consider the robotic system described by the constrained dynamic model (1) for the force design (4) and the control

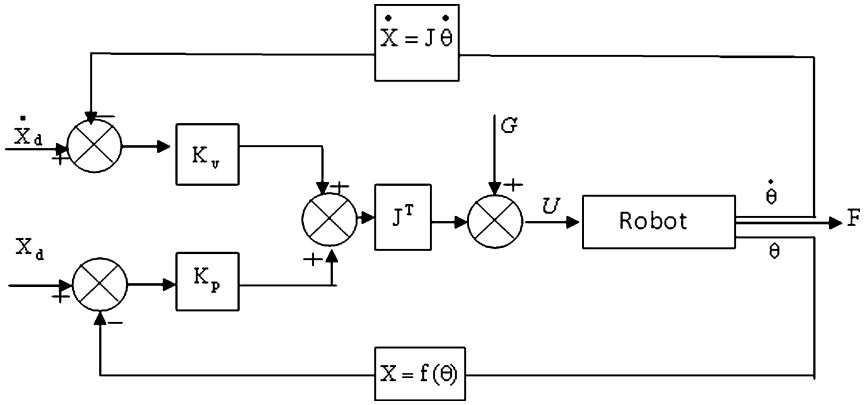

Fig. 1 Stiffness control concept [17]

law (3). Using the relations (5) and (6) we can write:

$$M(\Phi)\ddot{\Phi} + H(\Phi, \dot{\Phi}) + J^T(\Phi)KY(\Phi) + J^T(\Phi)K_v\dot{Y}(\Phi) = 0 \tag{7}$$

where:

$$K = K_p - K_e \tag{8}$$

In order to evaluate the relationship between the dynamics of the robotic system and its energy, we use Lagrange's equation described by [35]:

$$\frac{d}{dt}\left(\frac{\partial T}{\partial \dot{\Phi}}\right) - \frac{\partial T}{\partial \Phi} + \frac{\partial P}{\partial \Phi} + \frac{\partial D}{\partial \dot{\Phi}} = 0 \tag{9}$$

where $T(\Phi, \dot{\Phi})$ is the kinetic energy of the robotic system (1) defined by:

$$T(\Phi, \dot{\Phi}) = \frac{1}{2}\dot{\Phi}^T M(\Phi)\dot{\Phi} \tag{10}$$

$P(\Phi)$ and $D(\Phi, \dot{\Phi})$ are potential energy and dissipation function respectively. Comparing (7) and (9), we obtain the following relationship between the dynamics of the system and the energy terms $T(\Phi, \dot{\Phi})$, $P(\Phi)$ and $D(\Phi, \dot{\Phi})$ (see Appendix A):

$$\frac{\partial P(\Phi)}{\partial \Phi} = J^T(\Phi)KY(\Phi) \tag{11}$$

$$\frac{\partial D(\Phi, \dot{\Phi})}{\partial \dot{\Phi}} = J^T(\Phi)K_v\dot{Y}(\Phi) \tag{12}$$

$$H(\Phi, \dot{\Phi}) = \sum_{i=1}^{n}\left(\frac{d\Phi_i}{dt}\frac{\partial M}{\partial \Phi_i}\right)\frac{\dot{\Phi}}{2} \tag{13}$$

3.2 New Sufficient Stability Conditions for Stiffness Control

Let for the system (7) a Lyapunov Hamiltonian function defined by [35]:

$$V(\Phi, \dot{\Phi}) = T(\Phi, \dot{\Phi}) + P(\Phi) - P(0) \tag{14}$$

The error dynamics (7) are asymptotically stable if $V(\Phi, \dot{\Phi})$ satisfies the following conditions [36]:

$$V(0, 0) = 0 \quad \text{if } \Phi = 0, \dot{\Phi} = 0 \tag{15}$$

$$V(\Phi, \dot{\Phi}) > 0 \quad \text{if } \Phi \neq 0, \dot{\Phi} \neq 0 \tag{16}$$

$$\dot{V}(\Phi, \dot{\Phi}) < 0 \quad \text{if } \Phi \neq 0, \dot{\Phi} \neq 0 \tag{17}$$

Theorem 1 *If there exist diagonal matrices* $K_p, K_v, K_e \in R^{p\times p}$ *such that the following conditions*:

$$K_p - K_e > 0 \tag{18a}$$

$$K_v > 0 \tag{18b}$$

are satisfied, then the robotic system described by the dynamical model (1) *and the kinematic models* (2) *is asymptotically stable under the constrained force*:

$$F = K_e(X_d - X) \tag{19}$$

and the control law:

$$U = J^T[K_p(X_d - X) + K_v(\dot{X}_d - \dot{X})] + G \tag{20}$$

Proof See Appendix B. □

4 Impedance Control

Impedance control is a control strategy specifying a desired dynamic behavior for the robot. The robotic controller is designed to track a motion trajectory and realize a desired impedance dynamics between the end-effector position and the contact force [18, 19]. The desired impedance is defined by:

$$Z_d = \frac{F_d - F}{X_d - X} \tag{21}$$

where, X_d and F_d are desired Cartesian position and desired contact force, respectively. It is generally required that the

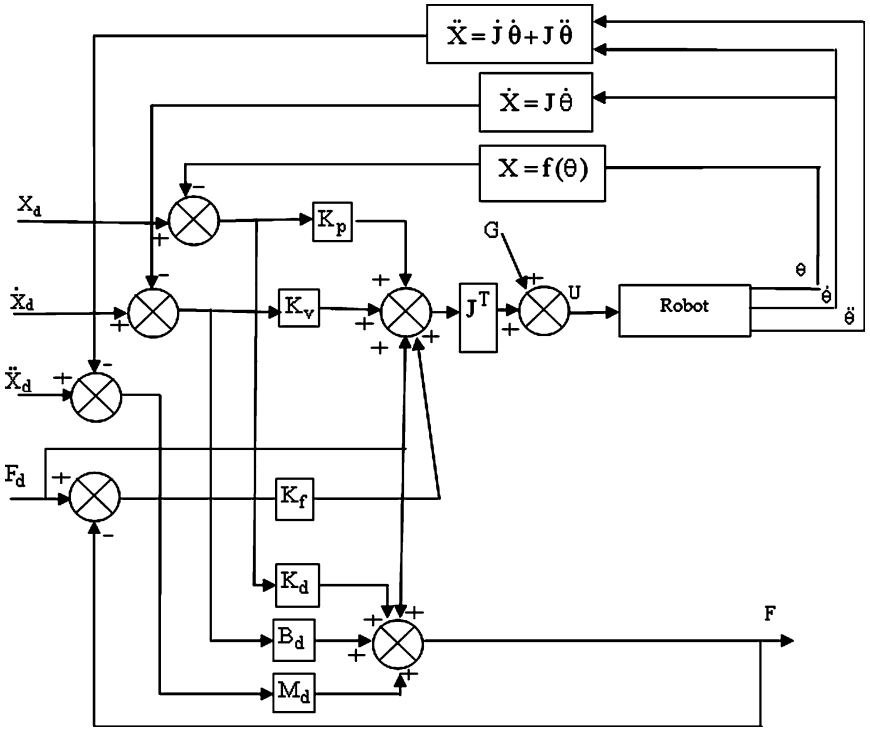

Fig. 2 Impedance control concept

desired impedance verifies [19]:

$$Z_d = K_d + B_d s + M_d s^2 \tag{22}$$

$K_d, B_d, M_d \in R^{p\times p}$ are desired stiffness, damping and inertia matrices and s is the Laplace operator. Substituting (21) in (22) gives:

$$F_d - F = K_d(X_d - X) + B_d(\dot{X}_d - \dot{X}) + M_d(\ddot{X}_d - \ddot{X}) \tag{23}$$

$\ddot{X} \in R^p$ is Cartesian end-effector acceleration where from (2b) we can write that $\ddot{X} = \dot{J}(\theta)\dot{\theta} + J(\theta)\ddot{\theta}$. The block diagram of the entire control system is shown in Fig. 2, where $K_p, K_v, K_f \in R^{p\times p}$ are position, velocity and force gain matrices, respectively. The control law is given by:

$$\begin{aligned} U = J^T[&K_p(X_d - X) + K_v(\dot{X}_d - \dot{X}) \\ &+ F_d(K_f + I) - K_f F] + G \end{aligned} \tag{24}$$

4.1 Relationship Between the Dynamics of the Robotic System and Its Energy for Impedance Control

Consider the robotic system described by the dynamic model (1) for the force design (23) and the control law (24). Using the relations (5) and (6) we can write:

$$\begin{aligned} &M(\Phi)\ddot{\Phi} + H(\Phi, \dot{\Phi}) + J^T(\Phi)K_1 Y(\Phi) \\ &\quad + J^T(\Phi)K_2\dot{Y}(\Phi) + J^T(\Phi)K_3\ddot{Y}(\Phi) = 0 \end{aligned} \tag{25}$$

where:

$$\begin{aligned} K_1 &= K_p + (I + K_f)K_d \\ K_2 &= K_v + (I + K_f)B_d \\ K_3 &= (I + K_f)M_d \end{aligned} \tag{26}$$

For the Lagrange equation (9) we can prove that (see Appendix C):

$$\frac{\partial P(\Phi)}{\partial \Phi} = J^T(\Phi)K_1 Y(\Phi) \tag{27}$$

$$\frac{\partial D(\Phi, \dot{\Phi})}{\partial \dot{\Phi}} = J^T(\Phi)K_2\dot{Y}(\Phi) + J^T(\Phi)K_3\ddot{Y}(\Phi) \tag{28}$$

$$H(\Phi, \dot{\Phi}) = \sum_{i=1}^{n}\left(\frac{d\Phi_i}{dt}\frac{\partial M}{\partial \Phi_i}\right)\frac{\dot{\Phi}}{2} \tag{29}$$

4.2 New Sufficient Stability Conditions for Impedance Control

Let for the error dynamics (25) a Lyapunov Hamiltonian function defined by (14). The system (25) is then asymptotically stable if $V(\Phi, \dot{\Phi})$ satisfies the Lyapunov conditions (15), (16) and (17).

Theorem 2 *For desired matrices $K_d, B_d, M_d \in R^{p\times p}$ and if there exist diagonal matrices $K_p, K_v, K_f \in R^{p\times p}$ such*

that the following conditions:

$$\begin{aligned} &K_p + (I + K_f)K_d > 0 \\ &K_v + (I + K_f)B_d > 0 \\ &M_d = 0 \end{aligned} \tag{30}$$

or

$$\begin{aligned} &K_p > 0 \\ &K_v > 0 \\ &K_f = -I \end{aligned} \tag{31}$$

are satisfied, then the robotic system described by the dynamical model (1) *and the kinematic models* (2) *is asymptotically stable under the constrained force*:

$$F = F_d - K_d(X_d - X) - B_d(\dot{X}_d - \dot{X}) - M_d(\ddot{X}_d - \ddot{X}) \tag{32}$$

and the control law:

$$\begin{aligned} U = J^T[&K_p(X_d - X) + K_v(\dot{X}_d - \dot{X}) \\ &+ K_f(F_d - F) + F_d] + G \end{aligned} \tag{33}$$

Proof See Appendix D [37]. □

5 Application

5.1 The Rehabilitation Situation

Repetitive functional training of the upper limb after stroke is essential to regain ordinary motion. Traditionally, this is achieved through manual one-on-one therapy which is physically exhausting for the therapist and expensive for the patients. A solution may be robotic rehabilitation or robot-aided therapy. Using robotic aided devices, a therapist is stay responsible for the nonphysical interaction and observation of the patient whereas the robotic device takes out the physical interaction with the patient. Indeed, robots have the ability to provide repetitive training movement and an objective quantitative assessment of movement [5–8].

In [38], we had already proposed a 2DOF end-point robot-aided rehabilitation. However, the robotic device neglects the motion of the shoulder girdle. Its end effector motion is then regrettably limited to linear trajectories.

In this paper, we propose a new design of a planar 3DOF rehabilitation device that allows the human upper limb to be trained with more realistic functional movements. Furthermore, to improve the function of the stroked upper limb, the robotic device must be attached to a human upper limb and must have joints lined with the upper limb joints in order to control them independently (see Fig. 3).

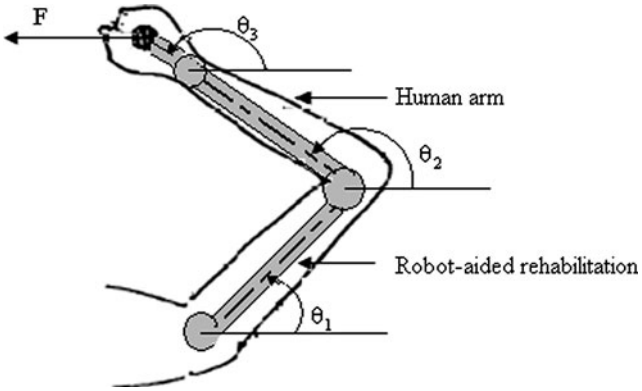

Fig. 3 Human arm attached to the 3DOF robot-aided rehabilitation

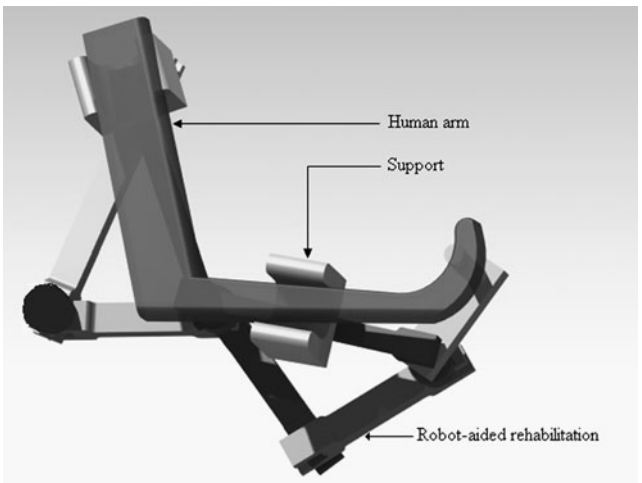

Fig. 4 3DOF robot-aided rehabilitation prototype

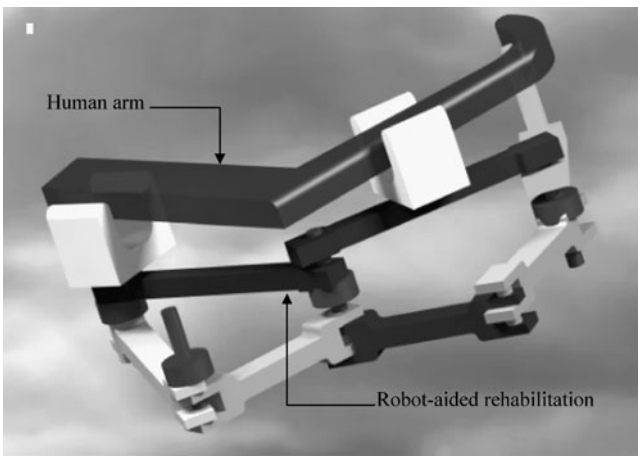

Fig. 5 Mechanical design of the 3DOF robot-aided rehabilitation

The mechanical system of the robot aided rehabilitation is composed by three parts (see Figs. 4 and 5): Three rigid bodies articulated by joints, two brackets and a linkage system. The brackets serve to maintain the upper limb of the

patient over the robot device and constraint it to move in parallel to the robot-aided rehabilitation. The linkage system allows the therapist to adjust distances between axes and customize the rehabilitation device for different users. The control system of the rehabilitation device is designed in order to authorize corrective forces and torques to the human arm. Desired positions are imposed by the rehabilitation aided robot whereas desired contact forces are imposed by the human arm.

5.2 The Human Arm

The physical parameters shown in Table 1 correspond to a right arm, forearm and hand of a stroked patient having a weight of 70 kg and a height of 1.73 m. They are computed using the famous Winter statistical model [39] and referring to [40]. The parameters m_i, L_i and k_i design mass, length and position of gravity center of each rigid body whereas The inertia parameters I_i $(i = 1, 2, 3)$ are computed using the relation:

$$I_i = \frac{m_i L_i^2}{12}$$

5.3 The Robot Aided Rehabilitation Model

The robot aided rehabilitation is a planar 3DOF robot. Its end-effector position $X = [x\ y]^T$ is computed using the following forward kinematic model:

$$\begin{cases} x = L_1 \cos\theta_1 + L_2 \cos\theta_2 + L_3 \cos\theta_3 \\ y = L_1 \sin\theta_1 + L_2 \sin\theta_2 + L_3 \sin\theta_3 \end{cases} \tag{34}$$

The matrices associated to dynamic model (1) and kinematic model (2b) are given by:

$$M(\theta) = \begin{bmatrix} I_1 + m_1 k_1^2 + m_2 L_1^2 + m_3 L_1^2 & a \cdot \cos(\theta_1 - \theta_2) & b \cdot \cos(\theta_1 - \theta_3) \\ a \cdot \cos(\theta_1 - \theta_2) & I_2 + m_2 k_2^2 + m_3 L_2^2 & c \cdot \cos(\theta_2 - \theta_3) \\ b \cdot \cos(\theta_1 - \theta_3) & c \cdot \cos(\theta_2 - \theta_3) & I_3 + m_3 k_3^2 \end{bmatrix}$$

$$H(\theta, \dot\theta) = \begin{bmatrix} 0 & a \cdot \sin(\theta_1 - \theta_2) & d \cdot \sin(\theta_1 - \theta_2) \\ -a \cdot \sin(\theta_1 - \theta_2) & 0 & c \cdot \sin(\theta_2 - \theta_3) \\ -d \cdot \sin(\theta_1 - \theta_2) & -c \cdot \sin(\theta_2 - \theta_3) & 0 \end{bmatrix} \begin{bmatrix} \dot\theta_1^2 \\ \dot\theta_2^2 \\ \dot\theta_3^2 \end{bmatrix}$$

$$G(\theta) = g \begin{bmatrix} (m_1 k_1 + m_2 L_1 + m_3 L_1) \cos\theta_1 \\ (m_2 k_2 + m_3 L_2) \cos\theta_2 \\ m_2 k_3 \cos\theta_3 \end{bmatrix}$$

$$J(\theta) = \begin{bmatrix} -L_1 \sin\theta_1 & -L_2 \sin\theta_2 & -L_3 \sin\theta_3 \\ L_1 \cos\theta_1 & L_2 \cos\theta_2 & L_3 \cos\theta_3 \end{bmatrix}$$

where:

$$a = m_2 L_1 k_2 + m_3 L_1 L_2$$

$$b = m_3 L_1 k_2$$

$$c = m_3 L_2 k_3$$

$$d = m_3 L_1 k_3$$

Furthermore, we assume that the robot-aided rehabilitation have the same parameters as the human arm given in Table 1.

5.4 Trajectory Generation

The desired Cartesian position, speed and acceleration of the robotic system are used as inputs of the control laws. So, it is important to generate desired trajectories. The motion must begin and end regularly such that:

$$\begin{aligned} &\theta_i(t_0) = \theta_{i0}; \qquad \dot\theta_i(t_0) = 0 \\ &\theta_i(t_f) = \theta_{id}; \qquad \dot\theta_i(t_f) = 0 \end{aligned} \tag{35}$$

where $i = 1, 2, 3$. So, we must choose, in the first stage, reference trajectories in the join space. We choose, in this work, three degree reference trajectories such that:

$$\theta_{i,d}(t) = a_{i0} + a_{i1} t + a_{i2} t^2 + a_{i3} t^3 \tag{36}$$

So, the desired joint velocities are deduced as:

$$\dot\theta_{i,d}(t) = a_{i1} + 2a_{i2} t + 3a_{i3} t^2 \tag{37}$$

where:

$$\begin{bmatrix} a_{i0} \\ a_{i1} \\ a_{i2} \\ a_{i3} \end{bmatrix} = \begin{bmatrix} 1 & t_0 & t_0^2 & t_0^3 \\ 1 & t_f & t_f^2 & t_f^3 \\ 0 & 1 & 2t_0 & 3t_0^2 \\ 0 & 1 & 2t_f & 3t_f^2 \end{bmatrix}^{-1} \begin{bmatrix} \theta_{i0} \\ \theta_{id} \\ 0 \\ 0 \end{bmatrix}$$

In the Cartesian space, we chose a circular profile. To realize this contour, we will introduce a sinusoidal signal on

Table 1 Human arm parameters

Bodies	m_i (kg)	L_i (m)	k_i (m)	I_i (kg m^{-2})
Arm	1.960	0.321	0.140	0.016
Forearm	1.120	0.253	0.109	0.006
hand	0.420	0.187	0.095	0.001

each axis. So, the axis references correspond to a harmony excitation in quadratic phase. Therefore, for a circle radius R, the desired end-effector motion of the robotic system will be defined by:

$$\begin{cases} x_d(t) = R\cos(a_{30} + a_{31}t + a_{32}t^2 + a_{33}t^3) \\ y_d(t) = R\sin(a_{30} + a_{31}t + a_{32}t^2 + a_{33}t^3) \end{cases} \tag{38}$$

For simulations, the movement of the trajectory is a circular motion with a radius of 0.76 m corresponding to the sum of arm, forearm and hand lengths aligned. We choose a movement beginning at $\theta_{i0} = [0\ 0\ 0]^T$ and ending at $\theta_{id} = [\pi\ \pi\ \pi]^T$ during 1 s ($t_0 = 0$ and $t_f = 1$ s). These parameters are chosen so that the human arm is in extension and the trajectory is a half of circle.

The desired trajectory of the end-effector of the robotic system is then deduced as:

$$\begin{cases} x_d(t) = 0.76\cos(3\pi t^2 - 2\pi t^3) \\ y_d(t) = 0.76\sin(3\pi t^2 - 2\pi t^3) \end{cases} \tag{39}$$

5.5 Results and Discussions

The goal of this section is to find optimal parameters for the control laws and force designs given by Theorems 1 and 2 for the rehabilitation situation described below. The optimization problem will be solved using the constrained nonlinear optimization method proposed in [41, 42] and solved using the *fmincon* function of the optimization toolbox of MatLab software. The dynamic and forward kinematic models are considered as nonlinear constrained equalities of the optimization problem whereas the stability conditions are considered as constrained inequalities. The dynamic model of the system is solved using the ODE45 solver of MatLab software.

5.5.1 Tuning Parameters of the Stiffness Approach

To adjust the parameters of the stiffness control law (20) and the constrained force design (19), the following nonlinear optimization problem is solved:

$$\min f(z) = \frac{1}{N}\sum_{i=1}^{N}\sqrt{E_i^2} \tag{40a}$$

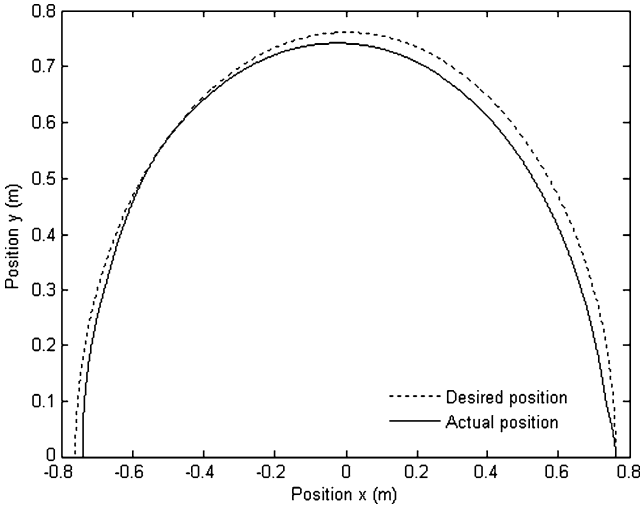

Fig. 6 End effector trajectory under stiffness control

subject to:

$$M(\theta)\ddot{\theta} + H(\theta,\dot{\theta}) + G(\theta) = U - J(\theta)^T F \tag{40b}$$

$$\dot{X} = J(\theta)\dot{\theta} \tag{40c}$$

$$\begin{bmatrix} -1 & 0 & 1 \\ 0 & -1 & 0 \end{bmatrix} z < \begin{bmatrix} 0 \\ 0 \end{bmatrix} \tag{40d}$$

$$100 \le k_p \le 700 \tag{40e}$$

$$30 \le k_v \le 400 \tag{40f}$$

$$1 \le k_e \le 20 \tag{40g}$$

where $z = [k_p\ k_v\ k_e]^T$ is the decision vector for the stiffness control strategy and $E_i = [X_d(i) - X(i)]^T$ is the trajectory error of the ith iteration. N is the iteration number. k_p, k_v and k_e are the diagonal elements of the gain matrices K_p, K_v and K_e, respectively. Relations (40b) and (40c) represent the dynamic and the kinematic constraints of the optimization problem whereas the inequality constraint (40d) is equivalent to the stability conditions (18a) and (18b). Inequalities (40e), (40f) and (40g) define a set of lower and upper bounds of the decision variables. To obtain simulation results, the optimization problem was solved for the initial decision vector $z_0 = [500\ 200\ 5]^T$.

Best decision vector and the corresponding objective function are reported in Table 2. Figure 6 shows the profile of the desired and actual trajectories. As can be seen, desired Cartesian trajectory is followed. Figures 7 and 8 shows contact forces and control laws, respectively.

5.5.2 Tuning Parameters of the Impedance Approach

To adjust the parameters of the impedance control law (33) and the constrained force design (32), the nonlinear optimization problem is solved for the objective function (40a)

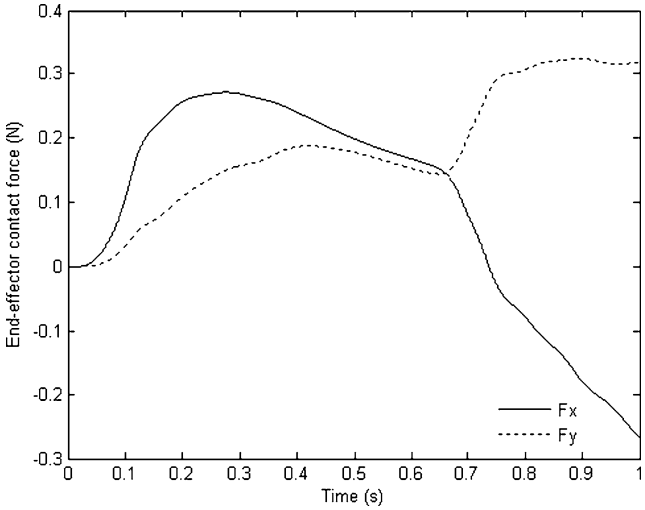

Fig. 7 Contact force response under stiffness control

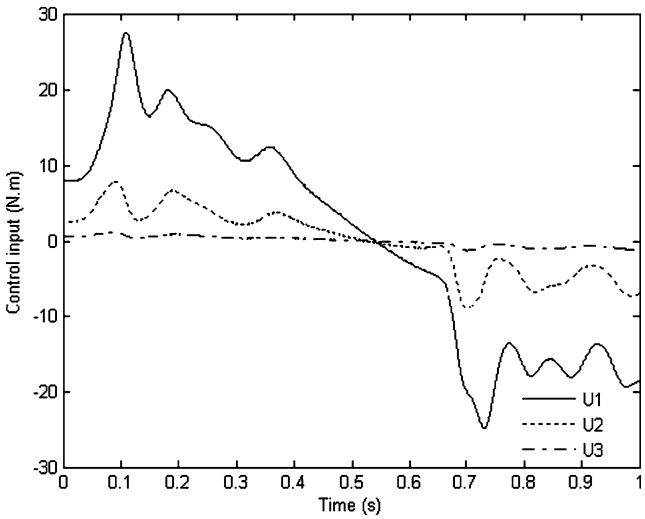

Fig. 8 Control laws under stiffness control

and the decision vector $z = [k_p\ k_v\ k_f]^T$ under the dynamic and the kinematic constraints (40b) and (40c), the inequality constraints:

$$\begin{bmatrix} -1 & 0 & -k_d \\ 0 & -1 & -b_d \end{bmatrix} z < \begin{bmatrix} k_d \\ b_d \end{bmatrix} \tag{41a}$$

$$100 \leq k_p \leq 700 \tag{41b}$$

$$30 \leq k_v \leq 400 \tag{41c}$$

$$1 \leq k_f \leq 50 \tag{41d}$$

and the equality constrains:

$$k_d = 20, \qquad b_d = 5, \qquad m_d = 0 \tag{41e}$$

where k_p, k_v, k_f, k_d, b_d and m_d are the diagonal elements of the gain matrices K_p, K_v, K_f, K_d, B_d and M_d, respectively.

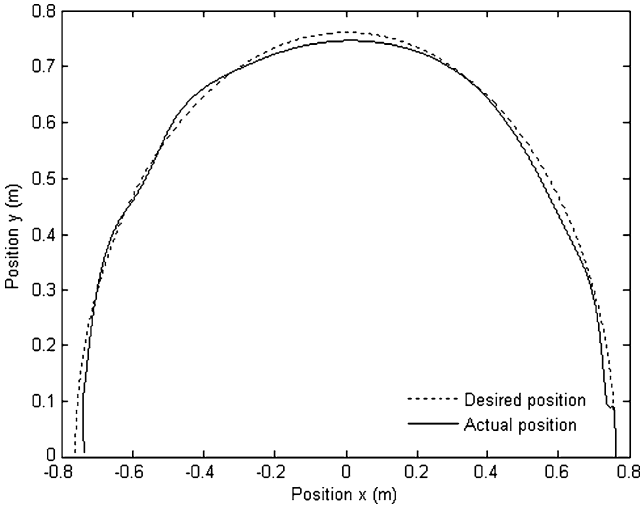

Fig. 9 End effector trajectory under impedance control

Table 2 Optimization strategy results

Control strategy	Decision vector	Objective function	Optimization time (s)
Stiffness control	$z = [550\ 350\ 9.3]^T$	0.03	620.3
Impedance control	$z = [650\ 235.3\ 25]^T$	0.017	831.9

In the last optimization problem, inequality (41a) with the equality constrains (41e) are equivalent to the stability conditions (30) for chosen impedance dynamics (22). Inequalities (41b), (41c) and (41d) define the set of lower and upper bounds of the decision variables.

To obtain simulation results, the optimization problem was solved for the initial decision vector $z_0 = [500\ 200\ 5]^T$ and the desired contact force $F_d = [6\ 0]^T$. Best decision vector and the corresponding objective function are reported in Table 2. Simulations are performed such that the end-effector of the robot track the circular desired position trajectory (39) and such that the end-effector contact force converge to the desired force F_d after one second. Figure 9 shows the movement of the end-effector who attempts to draw a half circle in horizontal plane. The path was more nearly circular. So, we can confirm that the desired trajectory was followed completely by the robotic device. On the other side, it can be seen in Fig. 10 that the error between the actual and desired forces becomes smaller with the progression of simulation time. Moreover, control laws shown in Fig. 11 are characterized by acceptable energetic profiles.

Based on results given in Table 2, it is clear that impedance control schema gives best objective function than stiffness control strategy. It guarantees then best system performances. Nevertheless it requires longer optimization time to tune control and force parameters.

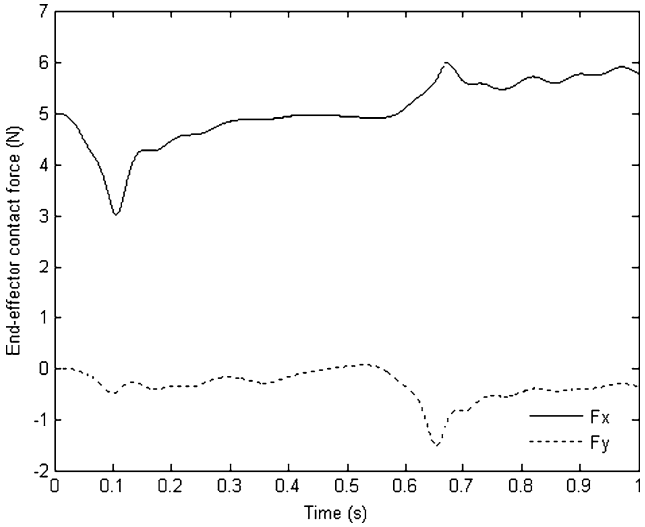

Fig. 10 Contact force response under impedance control

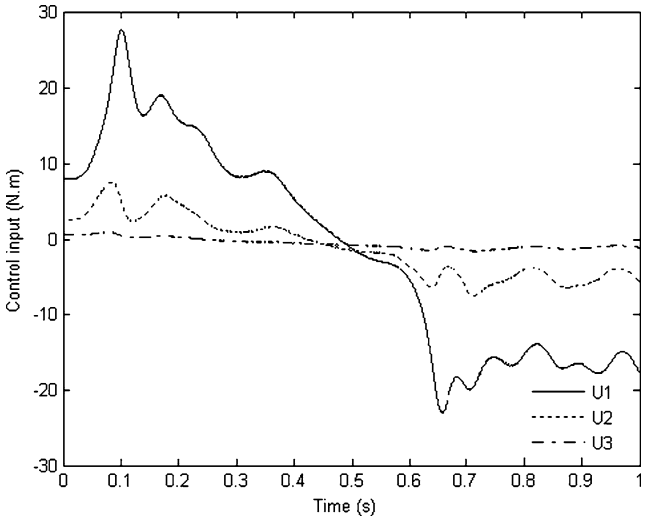

Fig. 11 Control laws under impedance control

5.5.3 Safety

It is clear that safety is firstly provided through hardware level. The therapist can adjust distances between axes and customize the rehabilitation device for different patients using the linkage system of the robotic device. Safety is also supplied through control software level. The robot is stopped when the stability conditions are not satisfied. The control system of the rehabilitation device is also designed in order to authorize corrective forces and torques to the human arm and to adapt controller laws on participant performances through suitable choice of stiffness parameter for the stiffness control approach and, stiffness, damping and inertia parameters for the impedance control approach.

5.5.4 Discussions

It is obvious that most famous upper limb rehabilitation devices are planar 2DOF arms while the shoulder joint is usually neglected [43–45]. To be trained with more realistic functional movements, current researches investigate in 3DOF robot-aided rehabilitation [46]. However, more interesting recent works focused on making devices portable so that they can be used during activities of daily living [47]. Such devices are more sophisticated, many degrees-of-freedom and support more complicated training movements. Furthermore, they can operate in the three dimensional space. However, it seems that is still even unclear whether robotic control approaches have the potential to produce better benefits and what control algorithms are most appropriate for which rehabilitation tasks [48]. That's why there is a great need, in the future, on control strategies that specify how the robot-aided therapy must interact with stroked patients. Performance-based, progressive robot-assisted therapy is also one of the most important prospects to be investigated [49, 50].

6 Conclusion

To improve the human arm function of stroked patients using robotic devices, a control strategy is proposed in this paper for monitoring robot-aided rehabilitation. The robotic device is controlled using an energy-based stiffness and impedance controllers for which new sufficient stability conditions are suggested. Some selecting controller parameters by the therapist can ensure adaptability and safety for patients at different stages of the therapy process whereas the remaining tuning parameters of the control strategies are adjusted using a constrained non linear optimization approach for which the stability conditions are considered as inequality constraints. A 3DOF planar robot-aided rehabilitation is used as a case study. The robotic device mimics the motion of the shoulder, elbow and wrist joints of user arm and it is configured for compliant motion in contact with a human upper limb. It was proven, by simulation results that desired trajectories are followed by the robotic device attached to the human arm. The functional training of a stroked upper limb could be then covered in motion and force.

To reduce the optimization time of the tuning of the controller parameters, we are currently analyzing, by simulation results, several biological-inspired optimization techniques known for their global convergence and good performances.

Future work will be addressed to the implementation and testing of control structures on a real application of a robot-aided rehabilitation. Different levels of disability interacting with the robot will be experimented. We will verify the effectiveness of the adjustment of control parameters to en-

sure a high level of capabilities such as adaptability to different patient disabilities, maximum level of safety in the interaction and flexibility to implement different motor tasks (passive mode, active-assisted mode and active-constrained mode). Hence, some specific actuators and an appropriate sensing system will be carefully designed and implemented to allow the robotic system to follow desired force and position safely and exactly. Finally, a Human-Machine Interface is also planned to help therapists and motivate patients during the treatment progress via the control strategy.

Appendix A: Relationship Between the Dynamics of the Robot and Its Energy (Stiffness Control Case)

Tacking on account that the inertia matrix $M(\Phi)$ is symmetric, we can write that:

$$\frac{\partial T}{\partial \dot{\Phi}} = M(\Phi)\dot{\Phi} \tag{A.1}$$

$$\frac{d}{dt}\left(\frac{\partial T}{\partial \dot{\Phi}}\right) = M(\Phi)\ddot{\Phi} + \sum_{i=1}^{n}\left(\frac{d\Phi_i}{dt}\frac{\partial M(\Phi)}{\partial \Phi_i}\right)\dot{\Phi} \tag{A.2}$$

$$\frac{\partial T}{\partial \Phi} = \frac{1}{2}\sum_{i=1}^{n} e_i \dot{\Phi}^T \left(\frac{\partial M(\Phi)}{\partial \Phi_i}\right)\dot{\Phi} \tag{A.3}$$

where n is the number of freedom of the robot and $e_i \in R^n$ is a unit vector. Using the relations (A.2) and (A.3) we have:

$$\frac{d}{dt}\left(\frac{\partial T}{\partial \dot{\Phi}}\right) - \frac{\partial T}{\partial \Phi} = M(\Phi)\ddot{\Phi} + \frac{1}{2}\sum_{i=1}^{n}\left(\frac{d\Phi_i}{dt}\frac{\partial M(\Phi)}{\partial \Phi_i}\right)\dot{\Phi} \tag{A.4}$$

Comparing (7) to (9) and using (A.4), the relation (13) is deduced. Since $\frac{dD}{d\dot{\Phi}}$ is equivalent to the term $J^T(\Phi)K_v\dot{Y}(\Phi)$ in the dynamic equation (7) so, the term $\frac{dP}{d\Phi}$ of Lagrange's equation corresponds to the term $J^T(\Phi)KY(\Phi)$.

Appendix B: Proof Theorem 1

Based on the Lyapunov function defined by the relation (14) and since $T(0,0) = 0$ and then $V(0,0) = 0$ so the first Lyapunov condition (15) is verified. To verify the second Lyapunov condition (16) and since the kinetic energy $T(\Phi, \dot{\Phi})$ is positive definite, it is sufficient to verify the positive definiteness of the following potential function:

$$V_p(\Phi) = P(\Phi) - P(0) \tag{B.1}$$

$V_p(\Phi)$ is positive definite if it is a convex function [35]. From (B.1) we have $V_p(0) = 0$. Based on (11) we can write:

$$\left[\frac{\partial V_p(\Phi)}{\partial \Phi}\right] = \left[\frac{\partial P(\Phi)}{\partial \Phi}\right] = J^T(\Phi)KY(\Phi) \tag{B.2}$$

we have then

$$\left[\frac{\partial V_p(\Phi)}{\partial \Phi}\right]_{\Phi=0} = J^T(0)KY(0) = 0 \tag{B.3}$$

In addition, let:

$$W = \frac{\partial}{\partial \Phi^T}\left(\frac{\partial \mathrm{V_p}(\Phi)}{\partial \Phi}\right) = \frac{\partial}{\partial \Phi^T}\left(\frac{\partial \mathrm{P}(\Phi)}{\partial \Phi}\right) \tag{B.4}$$

Substituting (B.2) in (B.4) we have:

$$W = \frac{\partial}{\partial \Phi^T}\left(J^T(\Phi)KY(\Phi)\right) = w_{ij} + J^T(\Phi)KJ(\Phi) \tag{B.5}$$

where

$$w_{ij} = \left(\frac{\partial J_i}{\partial \Phi_i}\right)^T KY(\Phi)$$

At the equilibrium point we have:

$$[W]_{\Phi=0} = J^T(0)KJ(0) \tag{B.6}$$

Thus function W is then positive definite at the equilibrium point if $K = K_p - K_e$ is positive definite. Hence the second Lyapunov condition (16) is satisfied if the condition (18a) is satisfied.

Using the expression (14) we have:

$$\frac{dV(\Phi, \dot{\Phi})}{dt} = \frac{dT(\Phi)}{dt} + \frac{dP(\Phi)}{dt} \tag{B.7}$$

From (10) we can write:

$$\frac{dT(\Phi, \dot{\Phi})}{dt} = \dot{\Phi}^T M\ddot{\Phi} + \dot{\Phi}^T \frac{dM}{dt}\frac{\dot{\Phi}}{2} = \dot{\Phi}^T M\ddot{\Phi} + H(\Phi, \dot{\Phi}) \tag{B.8}$$

Since

$$\frac{dP(\Phi)}{dt} = \dot{\Phi}^T \frac{\partial P}{\partial \Phi} \tag{B.9}$$

Substituting (11) in (B.9) we obtain:

$$\frac{dP(\Phi)}{dt} = \dot{\Phi}^T J^T(\Phi)KY(\Phi) \tag{B.10}$$

Substituting (B.8) and (B.10) in (B.7) we obtain:

$$\frac{dV(\Phi, \dot{\Phi})}{dt} = \dot{\Phi}^T M(\Phi)\ddot{\Phi} + \dot{\Phi}^T H(\Phi, \dot{\Phi})$$

$$+ \dot{\Phi}^T J^T(\Phi) K Y(\Phi) \tag{B.11}$$

From (7) we can write:

$$M(\Phi)\ddot{\Phi} + H(\Phi, \dot{\Phi}) + J^T(\Phi) K Y(\Phi) = -J^T(\Phi, \dot{\Phi}) K_v \dot{Y}(\Phi) \tag{B.12}$$

Substituting (B.12) in (B.11) gives:

$$\frac{dV(\Phi, \dot{\Phi})}{dt} = -\dot{\Phi}^T J^T(\Phi) K_v \dot{Y}(\Phi, \dot{\Phi}) \tag{B.13}$$

Using relations (2), (5) and (6) we obtain:

$$\frac{dV(\Phi, \dot{\Phi})}{dt} = -\dot{Y}^T(\Phi) K_v \dot{Y}(\Phi) \tag{B.14}$$

The third Lyapunov condition (17) is then satisfied K_v is positive definite.

Appendix C: Relationship Between the Dynamics of the Robot and Its Energy (Impedance Control Case)

Following the same steps as Appendix A by using the error dynamic model of the robotic system described by (25) instead of the model (7) used in the Appendix A, we can found that:

$$H(\Phi, \dot{\Phi}) = \frac{1}{2} \sum_{i=1}^{n} \left(\frac{d\Phi_i}{dt} \frac{\partial M(\Phi)}{\partial \Phi_i} \right) \dot{\Phi} \tag{C.1}$$

Since $\frac{dD(\Phi)}{d\dot{\Phi}}$ is equivalent to $J^T(\Phi) K_2 \dot{Y}(\Phi) + J^T(\Phi) K_3 \cdot \ddot{Y}(\Phi)$ term for the Lagrange model (9), so the term $\frac{dP(\Phi)}{d\Phi}$ is the same as the term $J^T(\Phi) K_1 Y(\Phi)$.

Appendix D: Proof Theorem 2

Using Appendix B, the first Lyapunov condition (15) is confirmed. The second Lyapunov condition (16) will be verified if we prove that $V_p(\Phi)$ is positive definite since the kinetic energy $T(\Phi, \dot{\Phi})$ is positive definite and $V_p(0) = 0$.

From (B.2) and (27) we can write:

$$\left[\frac{\partial V_p(\Phi)}{\partial \Phi} \right] = \left[\frac{\partial P(\Phi)}{\partial \Phi} \right] = J^T(\Phi) K_1 Y(\Phi) \tag{D.1}$$

then

$$\left[\frac{\partial V_p(\Phi)}{\partial \Phi} \right]_{\Phi=0} = J^T(0) K_1 Y(0) = 0 \tag{D.2}$$

Let consider the function W given by (B.4). Substituting (27) in (B.4) we have:

$$W = \frac{\partial}{\partial \Phi^T} (J^T(\Phi) K_1 Y(\Phi)) = w_{ij} + J^T(\Phi) K_1 J(\Phi) \tag{D.3}$$

where

$$w_{ij} = \left(\frac{\partial J_i}{\partial \Phi_i} \right)^T K_1 Y(\Phi)$$

At the equilibrium point we have:

$$[W]_{\Phi=0} = J^T(0) K_1 J(0) \tag{D.4}$$

Based on (D.4), the function W is positive definite at the equilibrium point if K_1 is positive definite. Hence the second Lyapunov condition (16) is satisfied if K_1 is positive definite. To prove the third Lyapunov condition (17), let substitute (27) in (B.9). This is gives:

$$\frac{dP(\Phi)}{dt} = \dot{\Phi}^T J^T(\Phi) K_1 Y(\Phi) \tag{D.5}$$

Substituting (B.8) and (D.5) in (B.7) we obtain:

$$\frac{dV(\Phi, \dot{\Phi})}{dt} = \dot{\Phi}^T M(\Phi)\ddot{\Phi} + \dot{\Phi}^T H(\Phi, \dot{\Phi}) + \dot{\Phi}^T J^T(\Phi) K_1 Y(\Phi) \tag{D.6}$$

From (25) we can write:

$$M(\Phi)\ddot{\Phi} + H(\Phi, \dot{\Phi}) + J^T(\Phi) K_1 Y(\Phi) = -(J^T(\Phi) K_2 \dot{Y}(\Phi) + J^T(\Phi) K_3 \ddot{Y}(\Phi)) \tag{D.7}$$

Substituting (D.7) in (D.6) gives:

$$\frac{dV(\Phi, \dot{\Phi})}{dt} = -\dot{\Phi}^T (J^T(\Phi) K_2 \dot{Y}(\Phi) + J^T(\Phi) K_3 \ddot{Y}(\Phi)) \tag{D.8}$$

Using relations (2), (5) and (6) gives:

$$\frac{dV(\Phi, \dot{\Phi})}{dt} = -\dot{Y}^T(\Phi)(K_2 \dot{Y}(\Phi) + K_3 \ddot{Y}(\Phi)) \tag{D.9}$$

The third Lyapunov condition (17) is then verified if K_2 is positive definite and K_3 is null. K_3 is null if: $I + K_f = 0$ or $M_d = 0$.

References

1. Masiero S, Celia A, Rosati G, Armani M (2007) Robotic-assisted rehabilitation of the upper limb after acute stroke. Arch Phys Med Rehabil 88(2):142–149. doi:10.1016/j.apmr.2006.10.032

2. Kwakkel G, Kollen BJ, Krebs HI (2008) Effects of robot-assisted therapy on upper limb recovery after stroke: a systematic review. Neurorehabil Neural Repair 22(2):111–121. doi:10.1177/1545968307305457
3. Kiguchi K, Kariya S, Watanabe K, Izumi K, Fukuda T (2001) An exoskeletal robot for human elbow motion support—sensor fusion, adaptation, and control. IEEE Trans Syst Man Cybern, Part B, Cybern 31(3):353–361. doi:10.1109/3477.931520
4. Papageorgiou X, McIntyre J, Kyriakopoulos KJ (2006) Towards recognition of control variables for an exoskeleton. In: Proceeding of the IEEE international symposium of intelligent control. doi:10.1109/CACSD-CCA-ISIC.2006.4777125
5. Stephen JB, Ian EB, Stephen HS (2007) A planar 3DOF robotic exoskeleton for rehabilitation and assessment. In: Proceeding of the 29th annual international conference of the IEEE EMBS. doi:10.1109/IEMBS.2007.4353216
6. Stephen JB, Ian EB, Stephen HS (2009) Performance evaluation of a planar 3DOF robotic exoskeleton for motor assessment. J Med Devices 3:1–12. doi:10.1115/1.3131727
7. Reinkensmeyer DJ, Aoyagi D, Emken JL, Galvez JA, Ichinose W, Kerdanyan G, Maneekobkunwong S, Minakata K, Nessler JA, Weber R, Roy RR, De Leon R, Bobrow JE, Harkema SJ, Edgerton VR (2006) Tools for understanding and optimizing robotic gait training. J Rehabil Res Dev 43:657–670. doi:10.1682/JRRD.2005.04.0073
8. Jan FV, Rik K, Edsko EGH, Ralf E, Edwin HFVA, Herman VK (2007) Design and evaluation of the LOPES exoskeleton robot for interactive gait rehabilitation. IEEE Trans Neural Syst Rehabil Eng 15(3):379–386. doi:10.1109/TNSRE.2007.903919
9. Prange GB, Jannink MJA, Groothuis-Oudshoorn CGM, Hermens HJ, Ijzerman MJ (2006) Systematic review of the effect of robot-aided therapy on recovery of the hemiparetic arm after stroke. J Rehabil Res Dev 43(2):171–183. doi:10.1682/JRRD.2005.04.0076
10. Krebs HI, Palazzolo JJ, Dipietro L, Ferraro M, Krol J, Rannekleiv K et al (2003) Rehabilitation robotics: Performance-based progressive robot-assisted therapy. Auton Robots 15(1):7–20. doi:10.1023/A:1024494031121
11. Linde RQVD, Lammertse P (2003) HapticMaster—a generic force controlled robot for human interaction. Ind Robot 30:515–524. doi:10.1108/01439910310506783
12. Soichi N, Ryojun I, Takahiro W, Kazuki M, Hideki S, Hitoshi H (2008) A study on impedance control using passive elements for human-assist system. In: Proceeding of the SICE annual conference. doi:10.1109/SICE.2008.46549722008
13. Krebs HI, Volpe BT, Aisen ML, Hogan N (2000) Increasing productivity and quality of care: robot-aided neurorehabilitation. J Rehabil Res Dev 37(6):639–652. http://bvs.insp.mx/articulos/2/8/03042001.pdf
14. Van der Kooij H, Veneman J, Ekkelenkamp R (2006) Compliant actuation of exoskeletons. In: Lazinica A (ed) Mobile robotics-towards new applications, Mammendorf. ISBN 978-3-86611-314-5
15. Vukobratovic MK, Tuneski A (1996) Adaptive control of single rigid robotic manipulators interacting with dynamic environment—an overview. J Intell Robot Syst 17:1–30. doi:10.1007/BF00435714
16. Raibert M, Craig JJ (1981) Hybrid position/force control of manipulators. J Dyn Syst Meas Control 120:126–133. doi:10.1115/1.3139652
17. Salisbury JK (1980) Active stiffness control of a manipulator in Cartesian coordinates. In: Proceeding of the IEEE international conference on decision and control including the symposium on adaptive processes. doi:10.1109/CDC.1980.272026
18. Hogan N (1984) Impedance control of industrial robots. Robot Comput-Integr Manuf 1:97–113. doi:10.1016/0736-5845(84)90084-X
19. Hogan N (1985) Impedance control: an approach to manipulators: Part 1, 2, 3. J Dyn Syst Meas Control 107:1–24. doi:10.1115/1.3140702
20. Chiaverini S, Sciavicco L (1993) The parallel approach to force/position control of robotic manipulators. IEEE Trans Robot Autom. doi:10.1109/70.246048
21. Kamnik R, Matko D, Bajd T (1998) Application of model reference adaptive control to industrial robot impedance control. J Intell Robot Syst 22:153–163. doi:10.1023/A:1007932701318
22. Sungchul K, Kiyoshi K, Kazuhito Y, Tetsuo K, Byungchan K, Shinsuk P (2010) Control of impulsive contact force between mobile manipulator and environment using effective mass and damping controls. Int J Precis Eng Manuf 11:697–704. doi:10.1007/s12541-010-0082-4
23. Vukobratovic MK, Rodić AG, Ekalo Y (1997) Impedance control as a particular case of the unified approach to the control of robots interacting with a dynamic known environment. J Intell Robot Syst 18:191–204. doi:10.1023/A:1007915307723
24. Chiaverini S, Siciliano B, Villani L (1999) A survey of robot interaction control schemes with experimental comparison. IEEE/ASME Trans Mechatron 4(3):273–285. doi:10.1109/3516.789685
25. Karunakar SB, Goldenberg AA (1988) Contact stability in model-based force control systems of robot manipulators. In: Proceeding of the IEEE international symposium on intelligent control. doi:10.1109/ISIC.1988.65467
26. Lawrence DA (1988) Impedance control stability properties in common implementation. In: Proceeding of the IEEE international conference on robotics and automation. doi:10.1109/ROBOT.1988.12222
27. Surdilovic D (1996) Contact stability issues in position based impedance control: theory and experiments. In: Proceeding of the IEEE international conference on robotics and automation. doi:10.1109/ROBOT.1996.506953
28. Kazerooni H, Waibel BJ, Kim S (1990) On the stability of robot compliant motion control: theory and experiments. J Dyn Syst Meas Control 112:417–426. doi:10.1115/1.2896159
29. Hogan N (1988) On the stability of manipulator performing contact tasks. IEEE J Robot Autom 4:677–686. doi:10.1109/56.9305
30. Tsumugiwa T, Yokogawa R, Yoshida K (2004) Stability analysis for impedance control of robot for human-robot cooperative task system. In: Proceedings of the IEEE/RSJ international conference on intelligent robots and systems. doi:10.1109/IROS.2004.1390020
31. Duchaine V, Gosselin CM (2008) Investigation of human-robot interaction stability using Lyapunov theory. In: Proceeding of the IEEE/RSJ international conference on robotics and automation. doi:10.1109/ROBOT.2008.4543531
32. Seul Jung Hsia TC (1999) Stability and convergence analysis of robust adaptive force tracking impedance control of robot manipulators. In: Proceedings of the IEEE/RSJ international conference on intelligent robots and systems. doi:10.1109/IROS.1999.812751
33. Buerger SP, Hogan N (2007) Complementary stability and loop shaping for improved Human–Robot interaction. IEEE Trans Robot 23:232–244. doi:10.1109/TRO.2007.892229
34. Zeng G, Hemami A (1997) An overview of robot force control. Robotica 15:473–482. doi:10.1017/S026357479700057X
35. Yabuta T, Chona AJ, Beni G (1988) On the asymptotic stability of the hybrid position/force control scheme for robot manipulators. In: Proceedings of the IEEE international conference on robotics and automation. doi:10.1109/ROBOT.1988.12071
36. Slotine JJE, Li W (1991) Applied nonlinear control. Prentice Hall, New York
37. Mehdi H, Boubaker O (2010) Position/force control for constrained robotic systems: a Lyapunov approach. In: Proceedings

of the IEEE international symposium on robotics and intelligent sensors. ISBN:978-4-9905048-0-9
38. Mehdi H, Boubaker O (2010) Rehabilitation of a human arm supported by a robotic manipulator: a position/force cooperative control. J Comput Sci 6(8):912–919. doi:10.3844/jcssp.2010.912.919
39. Winter DA (2009) Biomechanics and motor control of human movement. Wiley, New York
40. Aloulou A, Boubaker O (2010) Modeling and controlling a humanoid robot in the three dimensional space. In: Proceedings of the IEEE international symposium on robotics and intelligent sensors. ISBN:978-4-9905048-0-9
41. Gill PE, Murray W, Wright MH (1981) Practical optimization. Academic Press, San Diego
42. Powell MJD (1978) The convergence of variable metric methods for nonlinearly constrained optimization calculations. Academic Press, San Diego
43. Krebs HI, Hogan N, Aisen ML, Volpe BT (1998) Robot-aided neurorehabilitation. IEEE Trans Rehabil Eng 6(1):75–87. doi:10.1109/86.662623
44. Burgar CG, Lum PS, Shor PC, Machiel Van der Loos HF (2000) Development of robots for rehabilitation therapy: the Palo Alto VA/Stanford experience. J Rehabil Res Dev 37(6):663–673
45. Ju MS, Lin CCK, Lin DH, Hwang IS, Chen SM (2005) A rehabilitation robot with force position hybrid fuzzy controller: hybrid fuzzy control of rehabilitation robot. IEEE Trans Neural Syst Rehabil Eng 13(3):349–358. doi:10.1109/TNSRE.2005.847354
46. Jingguo W, Yangmin L (2010) A cooperated-robot arm used for rehabilitation treatment with hybrid impedance control method. In: Proceedings of the third international conference on intelligent robotics and applications. doi:10.1007/978-3-642-16587-0_42
47. Sugar TG, He J, Koeneman EJ, Koeneman JB, Herman R, Huang H et al (2007) Design and control of RUPERT: a device for robotic upper extremity repetitive therapy. IEEE Trans Neural Syst Rehabil Eng 15(3):336–346. doi:10.1109/TNSRE.2007.903903
48. Marchal-Crespo L, Reinkensmeyer DJ (2009) Review of control strategies for robotic movement training after neurologic injury. J NeuroEng Rehabil 6(1):6–20. doi:10.1186/1743-0003-6-20
49. Akdoğan E, Adli MA (2011) The design and control of a therapeutic exercise robot for lower limb rehabilitation: physiotherabot. Mechatronics 21(3):509–522. doi:10.1016/j.mechatronics.2011.01.005
50. Xu G, Song A, Li H (2011) Control system design for an upper-limb rehabilitation robot. Adv Robot 25(1–2):229–251. doi:10.1163/016918610X538561

Haifa Mehdi is a Ph.D. student under the supervision of Professor Olfa Boubaker at National Institute of Applied Sciences and Technology (INSAT). She received the Engineering Diploma and the Master Degree in Computer Science and Automatic Control from INSAT in 2008 and 2009, respectively. Her doctoral research explores the development of a theoretical framework to give sufficient stability conditions for safe and compliant control of robot-aided rehabilitation using Lyapunov theory. She also investigates in the expansion of bio-inspired optimization methods for tuning multivariable and nonlinear controllers.

Olfa Boubaker is a full Professor in Electrical Engineering and one of the founder of the Research Unit: Energy, Robotics, Control and Optimization at National Institute of Applied Sciences and Technology (INSAT). She received the Ph.D. degree in Electrical Engineering in 2000 from National Engineering school of Tunis (ENIT) and the Habilitation Universitaire degree in Control Engineering from National Engineering School of Sfax (ENIS) in 2007, respectively. Between 1996 and 2004, she was a permanent visitor of Laboratory of Analysis and Architecture of Systems (LAAS). Her research interests are focused on nonlinear and robust control theory and integrate applications in social robotics.